Cross-influence of toluene as tar model compound and HCl on Solid Oxide Fuel Cell anodes in Integrated Biomass Gasifier SOFC Systems

Cavalli, A.; Kunze, M.; Purushothaman Vellayani, Aravind

DOI
10.1016/j.apenergy.2018.09.060

Publication date
2018

Document Version
Final published version

Published in
Applied Energy

Applied Energy 231 (2018) 1–11

Contents lists available at ScienceDirect

Applied Energy

journal homepage: www.elsevier.com/locate/apenergy

Cross-influence of toluene as tar model compound and HCl on Solid Oxide Fuel Cell anodes in Integrated Biomass Gasifier SOFC Systems

A. Cavalli[a,*], M. Kunze[b], P.V. Aravind[a]

[a] Process & Energy Department, 3me Faculty, Delft University of Technology, Leeghwaterstraat 39, 2628 CB Delft, The Netherlands
[b] Institute of Energy and Process Systems Engineering, Technical University Braunschweig, Franz-Liszt-Straße 35, D-38106 Braunschweig, Germany

HIGHLIGHTS

- 82 ppmv HCl caused only an immediate and marginal increase in the cell ASR.
- Concentrations of toluene up to 8.4 g/Nm^3 did not cause cell performance degradation.
- Toluene seems to be partially reformed and oxidised inside the cell anode.
- Low concentrations of HCl seems to partially hinder toluene conversion in the cell.

ARTICLE INFO

Keywords:
Biomass gasifier
SOFC
HCl
Tar
Direct internal tar reforming
Contaminants cross-influence

ABSTRACT

Integrated Biomass Gasifier Solid Oxide Fuel Cell Systems represent an alternative to fossil fuel based power plants, and direct internal tar reforming allows achieving high efficiency and decreasing system complexity. However, at present, tar is removed or reformed externally since there is not yet general agreement on the fate of these compounds in the anode chamber, and no information is available on the combined effects of tar and other biosyngas contaminants. In this paper, we present the results of short-term experiments on the cross-influence of HCl and tar on Ni-GDC Solid Oxide Fuel Cell anode and on direct internal tar reforming. Initially, the cell was fed with humidified hydrogen and an increasing concentration of HCl (8, 42 and 82 ppmv) and toluene (2.5, 4.2 and 8.4 g/Nm^3) separately. Successively, 8.4 g/Nm^3 of toluene and an increasing concentration of HCl were fed to the cell. We used polarisation and power density curves, and outlet gas composition analysis to evaluate the contaminants effects. The presence of HCl and toluene caused only a marginal increase in the cell Area Specific Resistance (around 1.5% when the cell was operated at Open Circuit), and the Area Specific Resistance remained then constant during the exposure time. However, HCl affects tar reforming decreasing the concentration of CO_2 and CO at the cell outlet. The results indicate the feasibility of direct internal toluene reforming and suggest the revision of currently used tolerance limits based on contaminants cross-influence effects. Extensive research on this topic is still required.

1. Introduction

Great effort has been made in the past years to replace fossil fuels with clean, renewable and sustainable energy sources and fuels [1,2]. Among these, biomass has features closer to fossil fuels, but due to its low energy density and scattered distribution, it is necessary to develop small scale systems to fully exploit its potential in a clean and sustainable manner. In this regard, Integrated Biomass Gasifier Solid Oxide Fuel Cell Systems have received considerable attention for micro-CHP generation [3]. However, the removal of biosyngas contaminants, required to meet SOFCs tolerance limits, is a critical step for the success of this technology. The low overall efficiency caused by intermediate cooling steps necessary for gas cleaning, and complex process scheme might represent a barrier for the development of integrated biomass gasifier SOFC systems.

Hot gas cleaning and direct internal tar reforming are considered helpful to achieve high efficiency and decrease system complexity, thus allowing the development of efficient and cost-effective Integrated Biomass Gasifier Solid Oxide Fuel Cell Systems. In fact, hot gas cleaning helps to avoid the need for additional equipment and the thermodynamic penalty typical of cold gas cleaning, and direct internal tar reforming simplifies the system heat management and eliminates the

* Corresponding author.
E-mail address: a.cavalli@tudelft.nl (A. Cavalli).

https://doi.org/10.1016/j.apenergy.2018.09.060
Received 15 April 2018; Received in revised form 2 September 2018; Accepted 6 September 2018

Nomenclature

Acronyms

ASR	area specific resistance
CCS	carbon capture and storage
CHP	combined heat and power
DC	direct current
EIS	electrochemical impedance spectroscopy
GC	gas chromatograph
GDC	gadolinium-doped ceria
LSM	lanthanum strontium manganite
MFC	mass flow controller
OCV	open circuit voltage
PTFE	polytetrafluoroethylene
ScSZ	scandia stabilized zirconia
SEM-EDS	scanning electron microscope and energy dispersive X-ray spectroscopy
SOFC	solid oxide fuel cell
YSZ	yttria stabilized zirconia

Symbols

C_{in}	inlet carbon molar flow
C_{out}	outlet carbon molar flow
F	Faraday constant
i	current density
$P_{O_{2cat}}$	equilibrium oxygen partial pressure at cathode
$P_{O_{2ano}}$	equilibrium oxygen partial pressure at cathode
R	universal gas constant
T	temperature
V	voltage
V_{Nernst}	Nernst voltage

need of an external tar reformer [4]. Moreover, reforming reactions being endothermic, direct internal tar reforming reduces the need of excess cathode air to maintain constant the stack temperature thus increasing further the system efficiency.

Nonetheless, direct internal tar reforming might cause performance losses due to carbon deposition and even irreversibly damage the cell due to thermal and mechanical stress [5]. Additionally, depending on the operating conditions, high temperature gas cleaning is not suitable for decreasing contaminant concentrations below the ppmv levels. At these concentrations, other biosyngas contaminants, such as HCl, can reduce the performances of SOFCs [6] and they might have an impact on the catalytic reactions occurring in the anode chamber.

Direct internal tar reforming is not a new topic, and it has been investigated with both thermodynamic equilibrium calculations (e.g., [7,8]), and experimental work. Toluene is probably the most used model tar compound in literature. However, naphthalene [9–11], benzene [12,13], and real tar mixtures [14–17] have also been used. Baldinelli et al. studied the effect of 5 and 10 g/Nm^3 toluene in a simulated biosyngas mixture on Ni-YSZ. The tested concentration did not harm the cell and no carbon was observed in *post-mortem* analysis [18]. Also Madi et al. observed no significant added degradation when up to 4.1 g/Nm^3 toluene where fed to a Ni-YSZ cell operating on dry H_2, and even up to 14.4 g/Nm^3 when using simulated biosyngas [19]. Conversely, Liu et al. concluded that 6.3 g/Nm^3 toluene caused carbon deposition and worsened the performance of Ni-YSZ cells operated with biosyngas [20]. Papurello et al. observed a large decrease in performance when a Ni-YSZ cell was fed with simulated biosyngas and an amount of toluene as low as 0.1 g/Nm^3 [21,22]. This same model tar was used by Liu et al. with Ni-GDC cells. A toluene concentration of 20 g/Nm^3 did not degrade a cell operating under current with simulated biosyngas [23]. Also Doyle et al. investigated the effect of toluene on Ni-GDC using simulated biosyngas. Despite the deposition of carbon, as discovered with post-mortem SEM-EDS analysis, 20 g/Nm^3 actually increased the cell performance by decreasing the cell ASR and increasing the amount of fuel available due to the tar reforming. However, 32 g/Nm^3 dramatically affected the ASR even with a fuel utilisation close to 70% [24]. Namioka et al. reported a tolerance limit of 3 g/Nm^3 for a SOFC with Ni-ScSZ anode operated at 800 °C and 500 mA/cm^2 with humidified hydrogen and a steam to carbon ratio of 1. Interestingly, despite no carbon was observed at 10 g/Nm^3, disappearance of Ni particles was detected with SEM-EDS analysis [25]. The authors ascribed the observation to metal dusting corrosion, as explained in [26].

Also the effect of HCl contamination on SOFC anodes has been investigated in the past years [11,27–31]. Recently, Kuramoto et al. found that Ni-YSZ cells operated at 900 °C with a current density of 150 or 200 mA/cm^2 were not affected by the presence of 10 ppmv HCl when fed with simulated post-CCS syngas ($H_2/N_2/H_2O$ = 70.9/23.6/5.5 vol %) [32]. Similar results were obtained by Li et al. and Blesznowski et al. [33,34]. However, concentrations higher than 100 ppmv were reported to increase the cell degradation, especially with methane as fuel gas [35]. Conversely, Madi et al. reported more sever degradation when the cell was fed with H_2 rather than with syngas. They explained the observation by the decrease in HCl adsorption as due to competitive CO adsorption and oxidation. A degradation of 3.1% per 1000 h was observed already with 10 ppmv HCl in H_2 [36]. Papurello et al. showed that below 20 ppmv a cell fed with biogas reformate does not suffer degradation. Above this concentration, the loss in performance is probably caused by HCl adsorption on Ni [21].

Despite the presence of scientific work, at present there is not yet general agreement on the fate of tar in the anode chamber. This is due to the different anode materials tested, the discrepancies in the operating conditions, and the various model tar compounds used. Moreover, different diagnosis methodologies and techniques, and evaluation criteria might affect the conclusions of a study [37]. Regarding HCl, results are somewhat more congruent. However, the cross influence of HCl with tar and its effect on direct internal tar reforming has not been studied yet. This is a crucial issue since tolerance limit currently used in designing gasifier-SOFC systems are based on single contaminants effects.

Hot gas cleaning and direct internal tar reforming can improve system design, and therefore facilitate the development of Integrated Biomass Gasifier SOFC Systems. However, SOFC tolerance limits to HCl, tar, and their simultaneous presence are not yet well defined. For this reason, to the best knowledge of the authors, this paper presents for the first time in literature the results of experiments on the cross-influence of HCl and tar. Short-term tests with planar Ni-GDC SOFC using toluene as model compound and a mixture of humidified hydrogen and nitrogen as gas carrier were carried out to investigate the synergistic effect of HCl and tar on cell performances and on direct internal tar reforming.

2. Methodology

In this study, we used a mixture of humidified hydrogen and nitrogen as fuel gas. The absence of CO, CO_2 and CH_4 in the inlet fuel allowed to better evaluate the outlet amount of carbon containing compounds and, therefore, to observe the effect of HCl on tar reforming. The HCl concentration tested were 8, 42 and 82 ppmv. The lowest concentration was selected based on literature results reporting that up to 9 ppmv did not show any significant impact on hydrogen oxidation with Ni/GDC cells operated at 750 °C [11].

Toluene was selected as model tar. This compound has been used by various research groups since it is one of the most abundant tar species generated in downdraft gasifiers, it is more difficult to remove than heavier compounds when cold gas cleaning systems are used, and it is more reactive than polyaromatic tar compounds (e.g., naphthalene, pyrene, anthracene) [25,38,39]. Thermodynamic equilibrium calculations were performed using the software FactSage version 5.4.1 (Thermfact/CRCT, Montreal, Canada and GTT-Technologies, Aachen, Germany) to assure the cell was operated outside the possible carbon formation region. Taking as inputs the mass of the reactants, process temperature, and pressure the software gives as outputs the products and their amount based on Gibbs Free Energy minimization [40]. Toluene tested concentration were 2.5, 4.2 and 8.4 g/Nm^3, corresponding to 611, 1021 and 2059 ppmv.

In all the tests, the cell was operated at 750 °C and nearly atmospheric pressure. An anode flow rate of 1400 NmL/min composed of 33.0 vol% H_2, 4.2 vol% H_2O, and balance N_2 was used in the test. A cathode flow rate of 1800 NmL/min simulated air was used. The tests were repeated using another cell to confirm the results obtained.

2.1. Setup and equipment

The test station used in this study is illustrated in Fig. 1. A ceramic housing with ceramic anode inlet and outlet pipes was used for holding the cell inside an insulated furnace. Platinum gauzes were used on both anode and cathode sides for collecting current; the thickness of the anode current collector was 0.5 mm. The anode side was sealed using a squared gasket of Thermiculite^{TM} 866 0.5 mm thick while the cathode side was not sealed. To assure contact between electrodes and current collector, and to improve the sealing, a weight of 10 kg was placed on top of the ceramic housing. A planar electrolyte supported cell (H.C. Starck, Germany) with 100 µm thick electrolyte, 40 µm anode and 44 µm cathode was used. The anode was made of Ni-GDC and the cathode LSM mixed with 8YSZ; both electrodes had an area of 81 cm^2. The electrolyte was 8YSZ and had an area of 100 cm^2. The flow rates were regulated using mass flow controllers Bronkhorst EL-FLOW (Bronkhorst, The Netherlands). Steam was added to the fuel gas stream by bubbling the H_2 and N_2 mixture in a temperature controlled water bath (humidifier). It was assumed that the gas in the water bath was constantly in equilibrium with the liquid phase. Therefore, the steam content is a function of the liquid temperature, according to Antoine's equation. The line connecting the humidifier with the SOFC furnace was trace heated and kept at 125 °C. To add toluene, a fraction of the dry nitrogen mass flow was bubbled in a temperature controlled bath (tar evaporator) containing anhydrous toluene 99.8% (Sigma Aldrich, USA). Similar to the humidifier, the gas in the tar evaporator was assumed to be constantly in equilibrium with the liquid phase. This same system was already used in the past by Liu et al. and the accuracy of this assumption was verified by measuring the achievable concentration of toluene at the outlet of the tar evaporator [23]. To increase the concentration of toluene in the total anode gas, the flow rate of nitrogen passing through the evaporator was increased while the flow rate of nitrogen by-passing the tar evaporator was decreased. The temperature of the humidifier was adjusted to maintain constant the steam concentration in the total anode gas. The stainless steel pipes after the tar evaporator was trace heated to 125 °C. Hydrogen chloride was added using a gas bottle containing 300 ppmv of the contaminant in H_2 (Linde, Germany). A PTFE pipe was used for connecting the gas bottle with the MFC and this with the anode inlet as close as possible to the furnace to avoid any interaction with the stainless steel piping.

The cell performances were evaluated by means of polarisation (i-V) curves recorded using an external load PLZ603W (Kikusui Electronics Corp., Japan) and a DC power supply SM120–25D (Delta Elektronika B.V., The Netherlands). From the polarisation curve, the Area Specific Resistance (ASR) was calculated as the secant between two points, as illustrated in Eq. (1) below

$$ASR = \frac{\Delta V}{\Delta i} \tag{1}$$

where V is the voltage measured, and i the current density drawn from the cell. Only the linear-behaviour section of the polarisation curve was considered, corresponding to a current density of 0.01 A/cm^2 and 0.24 A/cm^2. The Open Circuit Voltage (OCV) measured were compared with the Nernst voltages calculated using Eq. (2) below

$$V_{Nernst} = \frac{RT}{4F}\ln\left(\frac{P_{O_{2cat}}}{P_{O_{2ano}}}\right) \tag{2}$$

where R is the universal gas constant, T is the cell operating temperature, F is the Faraday constant and P_{O2} the equilibrium oxygen partial pressure at cathode and anode sides calculated using FactSage.

The behaviour of toluene in the anode chamber was evaluated by monitoring the outlet gas composition using a microGC Agilent 490 with a CP-Molsieve 5 Å capillary for measuring CO, H_2, N_2 and CH_4 and a PoraPlot U capillary for measuring CO_2 (Agilent, USA). Before reaching the microGC, the gas was passed through a condenser and a desiccator containing silica-gel to remove the moisture contained in the gas. The anode outlet flow rate was back-calculated from the inlet N_2 flow rate and the N_2 outlet concentration measured with the microGC. This was then used to calculate the flow rates of H_2, CO, CO_2 and CH_4. The values are based on the average of the last 5 gas samples analysed by the microGC. The results are used for a qualitative analysis of the trends observed at different operating conditions.

2.2. Testing procedure

The cell was heated up to 800 °C, with a ramp of 30 °C/hour to avoid excessive thermal stress. A flow rate of 1600 NmL/min N_2 and 1800 NmL/min simulated air was maintained at anode and cathode, respectively. The cell was reduced by stepwise increasing the H_2 content of the anode flow rate over a period of 4 h. The cell temperature was then increased to 950 °C and maintained for 12 h. The anode flow rate was then set to 1250 NmL/min H_2 with 4.2% H_2O and a polarisation curve was recorded to check the successful reduction of the cell. Another i-V curve was recorded with the gas composition to be used in the tests with HCl and toluene, that is 1400 NmL/min with 33.0% hydrogen, 4.2% steam and balancing nitrogen. The cell temperature was then lowered to 750 °C and two polarisation curves were recorded with these same gas compositions. This last curve was used as reference for

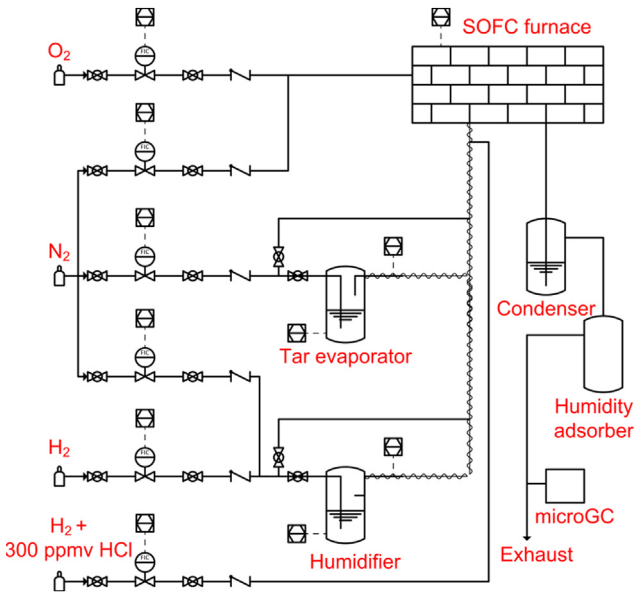

Fig. 1. Scheme of the test station.

the first HCl concentration tested. A reference polarisation curve was recorded each day of testing to take into account self-degradation of the cell.

The lowest concentration of HCl, that is 8 ppmv, was then added to the anode flow rate while the cell was at OCV. A polarisation curve was recorded two minutes after the addition of the contaminant, that is approximatively 10 times the minimum time required for the HCl-containing gas to travel from the mass-flow controller to the cell. A polarisation curve was recorded after 30 min of exposure to HCl while keeping the cell at OCV. Successively, a current of 0.08 A/cm^2 was drawn from the cell and after 30 min of exposure to HCl a new polarisation curve was recorded. The other HCl concentrations were successively tested following the same methodology as above. Fig. 2 shows the testing procedure followed for the first concentration of HCl tested.

After keeping the cell at OCV with 5% H_2 and balance N_2 for two days, a new reference curve was recorded to be used for the tests with toluene. In this case, one curve was recorded two minutes after the addition of the contaminant, and one after 60 min of exposure keeping the cell at 0.08 A/cm^2. If no degradation was observed, the cell was exposed to toluene for 60 min at OCV and a new polarisation curve was recorded at the end of this period. The exposure time was increased in order to have a stable gas composition at the cell outlet since the silica gel used to remove moisture also adsorbs CO_2 [41]. Since current is reported to be a preventive measure for carbon accumulation, the test was first done under current and, if no significant negative effect was observed, also at OCV [8]. The other toluene concentrations were successively tested following the same methodology.

A new reference test was carried out before proceeding with the combined effect of HCl and toluene. Also in this case, one curve was recorded two minutes after adding the contaminants, a second curve after 60 min of exposure keeping the cell at 0.08 A/cm^2, and a final one after 60 min of exposure with the cell at OCV. The other HCl concentrations were successively tested in the same manner and keeping the amount of toluene equal to 8.4 g/Nm^3. Table 1 summarises the tests performed and the relevant operating conditions.

Table 1
Synoptic table summarising the tests performed and the relevant parameters.

Test #	HCl concentration (ppmv)	Toluene concentration (g/Nm^3)/(ppmv)	Operating conditions	Duration (min)
1	8	0	OCV	30
2	8	0	0.08 A/cm^2	30
3	42	0	OCV	30
4	42	0	0.08 A/cm^2	30
5	82	0	OCV	30
6	82	0	0.08 A/cm^2	30
7	0	2.5/611	0.08 A/cm^2	60
8	0	2.5/611	OCV	60
9	0	4.2/1021	0.08 A/cm^2	60
10	0	4.2/1021	OCV	60
11	0	8.4/2059	0.08 A/cm^2	60
12	0	8.4/2059	OCV	60
13	8	8.4/2059	0.08 A/cm^2	60
14	8	8.4/2059	OCV	60
15	42	8.4/2059	0.08 A/cm^2	60
16	42	8.4/2059	OCV	60
17	82	8.4/2059	0.08 A/cm^2	60
18	82	8.4/2059	OCV	60

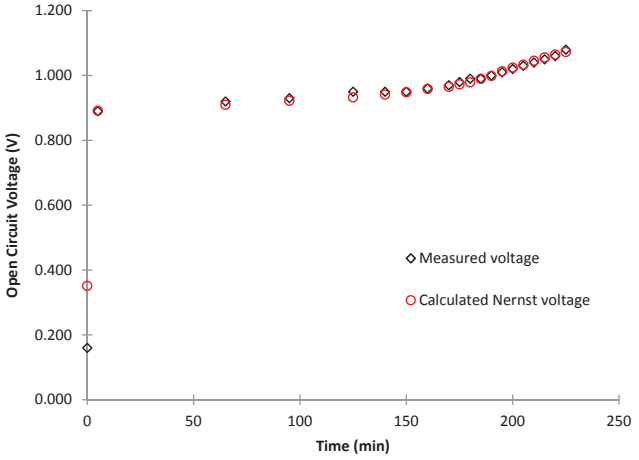

Fig. 3. Comparison between OCV measured and calculated during anode reduction at 800 °C.

3. Results and discussion

Fig. 3 shows the Nernst voltage calculated and the OCV measured during the reduction procedure. Excluding the first value, which was measured before starting the reduction procedure, the maximum deviation between measured and calculated values is lower than 2%, thus indicating a satisfactory sealing of the setup.

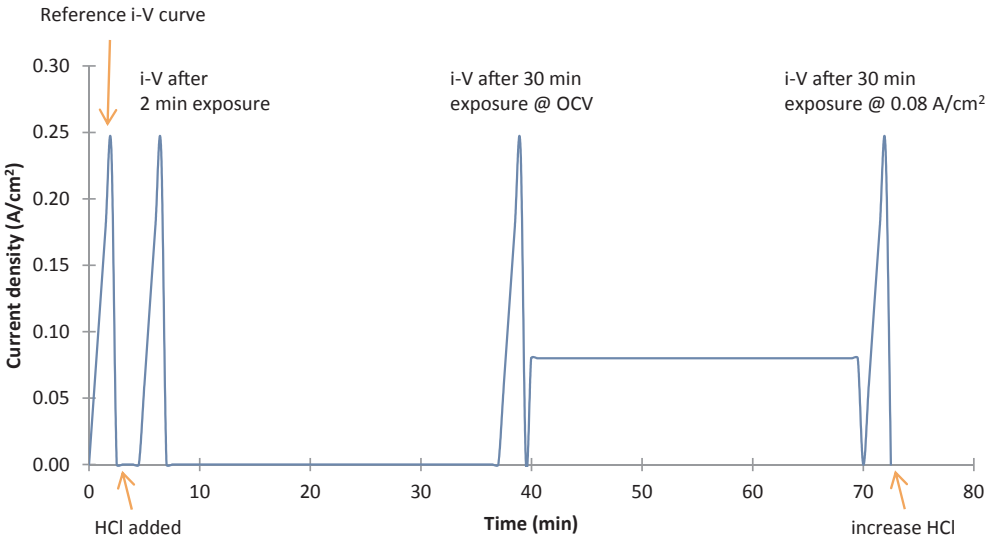

Fig. 2. Example of the testing procedure followed for the first concentration of HCl tested.

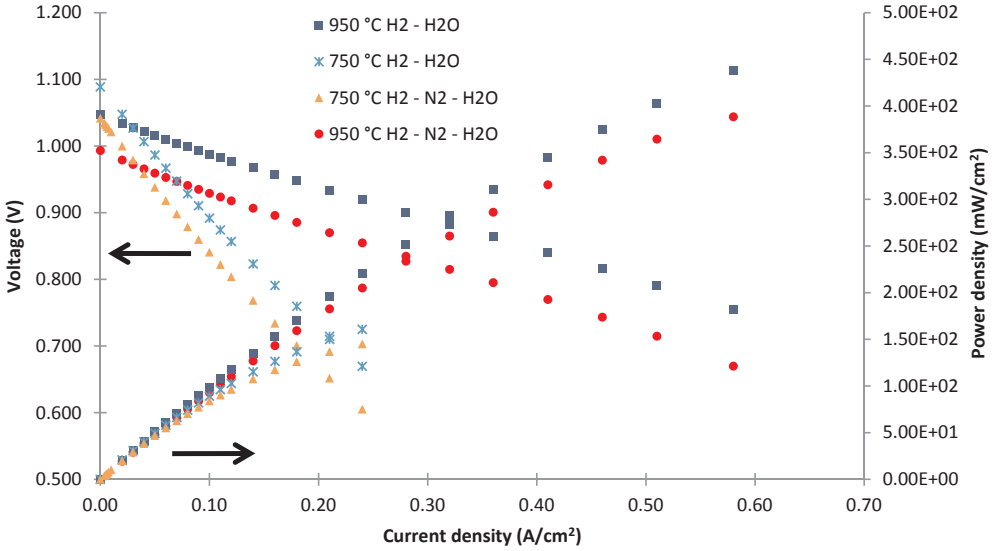

Fig. 4. Polarisation and power density curves of the cell operating at 950 °C and 750 °C with two different anode gas compositions.

Fig. 4 shows polarisation and power density curves measured for checking the cell performances. Table 2 reports a summary of the most important parameters, that is measured OCV and calculated Nernst voltage, ASR and power density at 0.24 A/cm^2 current. The polarisation curves recorded at the same temperature but different gas composition were almost parallel. The power density decreased when H_2 was diluted with N_2 from 221 to 205 mW/cm^2 at 950 °C. The ASR increased markedly from 0.57 Ω * cm^2 at 950 °C to 1.81 Ω * cm^2 at 750 °C. Below approximatively 0.03 A/cm^2, the cell voltage was higher at lower operating temperature. In all the conditions tested, the shape of the current-voltage curves indicated that ohmic losses seemed the dominant contribution to the ASR. This is analogous to what observed by Liu et al. using a comparable setup [23].

3.1. Effect of HCl

The first concentration of HCl tested (8 ppmv) showed no significant impact on the cell ASR and power density after 2 min from the injection and after 30 min of exposure at OCV or under current. Table 3 presents the ASR and the power density measured after the exposure keeping the cell at 0.24 A/cm^2.

The variation in both ASR and power density were less than 1% with the tested concentration of HCl. The results are in agreement with [32,21,33,34,11], and confirm that an HCl concentration of 8–10 ppmv does not affect the cell performance when H_2 is the anode fuel gas. The ASR measured after keeping the cell with 0.08 A/cm^2 was slightly lower (around 1.5%) than the reference case. This might have been caused by a minimal increase in the local cell temperature due to the current flow, and that was not detectable with the thermocouple. In fact, an increase in the cell temperature of only 2 °C can cause a decrease in the ASR of a solid oxide cell of 1–2% [42]. Such modest variations in the cell temperature are not easily measured by the thermocouple that was placed inside the ceramic housing. Likewise, also 42 ppmv HCl did not affect the cell negatively, in agreement with what was reported by Bao et al.

Table 3
ASR and power density measured when 8 ppmv HCl are added to the anode gas, and after 30 min of exposure at OCV and under current.

	ASR (Ω * cm^2)	Power density@0.24 A/cm^2 (mW/cm^2)
Clean gas	1.81	1.45E + 02
After injection	1.81	1.45E + 02
After 30 min@OCV	1.80	1.45E + 02
After 30 min@0.08 A/cm^2	1.78	1.46E + 02

[29]. Conversely, the cell ASR rose when the contaminant concentration was increased to 82 ppmv. However, this increase was only marginal and in the order of 1.5% after the cell was maintained at OCV during the exposure and 0.5% after the cell was kept under current. Moreover, the decrease was observed right after the introduction of the contaminant and did not get worse with time. Fig. 5 shows polarisation and power density curves before and after the exposure to 82 ppmv HCl keeping the cell at OCV. For currents lower than 0.12 A/cm^2 the voltage was higher after the exposure to HCl (black asterisks are slightly on top of the red dots). This might have been due to a minimally higher concentration of H_2 caused by the different accuracies of the MFCs used. In fact, while for H_2 a MFC with an accuracy of ± (0.5% read value + 0.1% full scale) was used, for the gas mix HCl + H_2 a MFC with accuracy of ± 1% full scale was used.

The slight performance drop due to the presence of 82 ppmv HCl might have been caused by HCl adsorbed on Ni, thus reducing the availability of active sites for H_2 reduction, as suggested by Trembly et al. [43]. The effect was not severe, in accordance with the results of Haga et al., who observed a decrease in performance of 0.017% per hour [30]. The larger effect observed in our test (0.5–1.5% ASR increase) might have been caused by the lower cell operating temperature and the presence of N_2 diluting the H_2 stream. Also Marina et al. observed performance degradation with similar HCl levels, although the

Table 2
Comparison of performance at different operating conditions.

Temperature (°C)	Gas composition	Measured OCV (V)	Nernst voltage (V)	Deviation (%)	ASR (Ω * cm^2)	Power density@0.24 A/cm^2 (mW/cm^2)
950	H_2 – H_2O	1.048	1.058	−0.9	0.52	2.21E + 02
950	H_2 – N_2 – H_2O	0.993	1.002	−0.9	0.57	2.05E + 02
750	H_2 – H_2O	1.089	1.095	−0.6	1.72	1.61E + 02
750	H_2 – N_2 – H_2O	1.042	1.049	−0.7	1.81	1.45E + 02

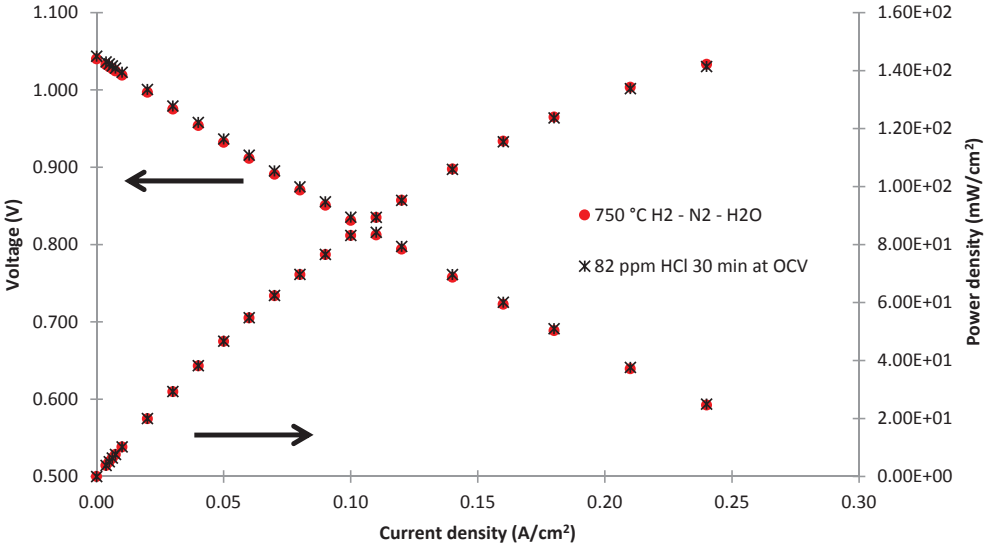

Fig. 5. Cell performance after exposure to 82 ppmv HCl for 30 min at OCV.

increase in the cell series resistance was much higher and equal to roughly $0.15\,\Omega * cm^2$ [27].

In summary, the highest concentration of HCl tested, that is 82 ppmv, caused an increase in the cell ASR. This increase was only marginal and in the range of 1.5% after the cell was kept at OCV, and 0.5% after the cell was kept under current. Moreover, the effect of the contaminant was observed as soon as the contaminant reached the cell anode and the ASR remained then constant during the exposure time. HCl concentrations as high as 82 ppmv are therefore believed not to significantly affect Ni-GDC short-term performance when the cell is fed with H_2.

Hydrogen chloride concentration in biosyngas depends on the feedstock used and it varies between 2 and 200 ppmv for verge grass and demolition wood, respectively, and can reach up to thousands ppmv when straw is used as fuel [44,45]. At high temperature, HCl can be removed using sorbents based on alkali metals and alkali earth metals. According to Krishna et al., when sodium or potassium based sorbents are used, the equilibrium partial pressure of HCl in coal derived syngas is less than 1 ppmv at 500 °C [46]. The concentration of steam and CO_2 should be taken into account when selecting a sorbent for HCl removal since they are among the products of the chemisorption reaction and, therefore, they affect the residual HCl concentration. Eq. (3) below illustrates the chemisorption reaction when sodium carbonate is used as sorbent.

$$Na_2CO_3 + 2HCl \leftrightarrow 2NaCl + H_2O + CO_2 \quad (3)$$

Based on the results obtained and on the tolerance limits found in literature, it might appear that HCl does not always require a significant cleaning effort. This implies a simplified gas cleaning section or an HCl removal reactor operating above 500 °C. However, these results are based on the effect of HCl as the only contaminant, and not on cross-influence studies. Furthermore, at high temperature (above 500 °C), the concentration of the metal chloride formed in the cleaning step starts to be above the ppmv level and might harm downstream equipment [46]. Moreover, large quantities of HCl might cause corrosion in other downstream equipment, especially in the heat recovery section of a micro-CHP system. Therefore, the implications of having a gas cleaning unit operating above 500 °C should be analysed not only at cell but also at system level.

3.2. Effect of tar

Table 4 shows the cell open circuit voltage measured and the Nernst voltage calculated for the different concentrations of toluene used in the test. The OCV reported is the one measured after 60 min of exposure to toluene keeping the cell at open circuit. As proposed by Mermelstein et al., the increase in OCV can be due to internal catalytic decomposition and/or reforming of the tar, but also to the direct oxidation of the tar or of the deposited carbon, which might affect the OCV since they have a different thermodynamic standard potential than H_2 [13]. The deviation between expected and measured value increased with the toluene content. The higher flow rate of nitrogen passed in the tar evaporator to increase toluene concentration in the total anode gas might have reduced the accuracy of the assumption of equilibrium between toluene liquid and gaseous phase. On the other hand, Nernst voltage was calculated assuming equilibrium of the gas compounds present in the anode chamber and this assumption also might be not accurate, especially when higher concentrations of toluene were used. A similar explanation was given by Baldinelli et al., who measured a voltage increase lower than expected when replacing H_2 and CO with CH_4. They ascribed the observation to a non-complete reforming of methane [18]. Moreover, Doyle et al. detected unconverted toluene at the cell outlet in experiments carried out with a similar setup, thus confirming that part of the toluene might have been not converted [24].

The ASR and the power density calculated with the different concentrations of toluene are presented in Table 5. With all the concentration of toluene tested, there was no noticeable increase in the ASR. Also in this case, after keeping the cell under current for 60 min, the cell ASR decreased. Fig. 6 shows polarisation and power density curves of the cell before and after the exposure to 8.4 g/Nm^3 toluene at OCV and under 0.08 A/cm^2 current. The decrease in ASR after exposure to toluene keeping the cell under current can be noticed from the larger voltage difference between reference case and toluene containing cases

Table 4
Comparison of theoretical and measured OCV with different toluene concentrations.

	Measured OCV (V)	Nernst voltage (V)	Deviation (%)
750 °C $H_2 - N_2 - H_2O$	1.041	1.049	−0.8
2.5 g/Nm^3 611 ppmv toluene	1.043	1.055	−1.1
4.2 g/Nm^3 1021 ppmv toluene	1.046	1.059	−1.3
8.4 g/Nm^3 2059 ppmv toluene	1.051	1.072	−2.0

Table 5
ASR and power density measured when the different concentrations of toluene are added to the anode gas, after 60 min of exposure at OCV and under current.

		ASR ($\Omega * cm^2$)	Power density@ 0.24 A/cm^2 (mW/cm^2)
Clean gas		2.04	1.31E + 02
After 60 min@ OCV	2.5 g/Nm^3 (611 ppmv)	2.04	1.32E + 02
After 60 min@ 0.08 A/cm^2	toluene	1.98	1.35E + 02
After 60 min@ OCV	4.2 g/Nm^3 (1021 ppmv)	2.03	1.33E + 02
After 60 min@ 0.08 A/cm^2	toluene	1.98	1.36E + 02
After 60 min@ OCV	8.4 g/Nm^3 (2059 ppmv)	2.04	1.34E + 02
After 60 min@ 0.08 A/cm^2	toluene	2.00	1.36E + 02

at zero current and at 0.24 A/cm^2. It is reported in literature that carbon deposition has the ability to improve electrical conductivity of the anode [47]. However, if the decrease in ASR was due to carbon deposition, this should have been observed after keeping the cell at OCV as well. Moreover, according to thermodynamic equilibrium calculation, even at OCV the cell was operating outside the carbon formation region. Therefore, it is more probable that the decrease in ASR was due to a minor increase in the cell temperature, as observed in the case of HCl. Fig. 7 shows the C-H-O ternary diagram with the line separating the carbon formation region at 750 °C.

As expected, due to the larger quantity of fuel available at the cell anode, the power density increased as illustrated in Fig. 8, where the power density generated at 0.24 A/cm^2 is shown as a function of the toluene content.

Despite the different testing conditions, the results obtained are in agreement with literature [18,23,24]. Madi et al. indicated only 4.1 g/Nm^3 toluene as the tolerance limit, but in their tests dry H_2 was used [19]. The highest concentration of toluene (8.4 g/Nm^3) that did not cause drop in the cell performance is partially higher than that indicated by Liu et al. and even two orders of magnitude higher than that indicated by Papurello et al. [20,21]. However, in their studies toluene

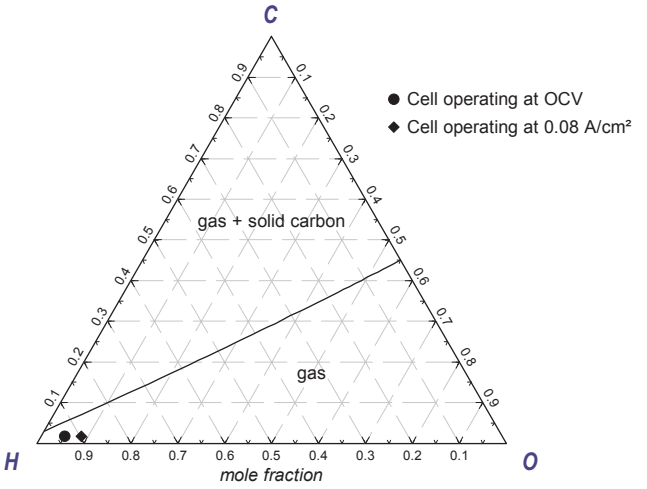

Fig. 7. C-H-O ternary diagram indicating the carbon formation region at 750 °C and the operating conditions when 8.4 g/Nm^3 toluene were added.

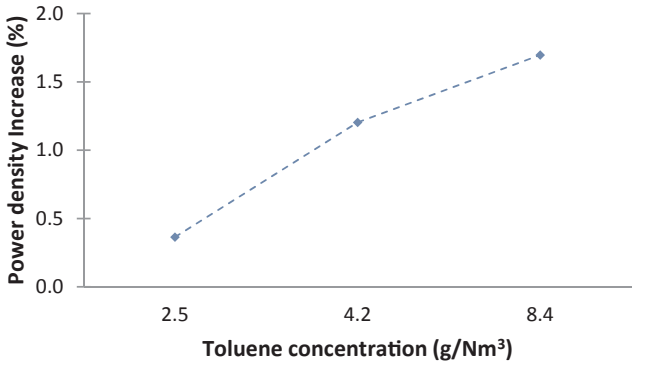

Fig. 8. Increase in power density at 0.24 A/cm^2 after keeping the cell at OCV for 60 min.

was carried by simulated biosyngas; therefore, other reactions might have contributed to carbon deposition. Moreover, they have studied Ni-YSZ cells, and ceria is reported to help the gasification of deposited

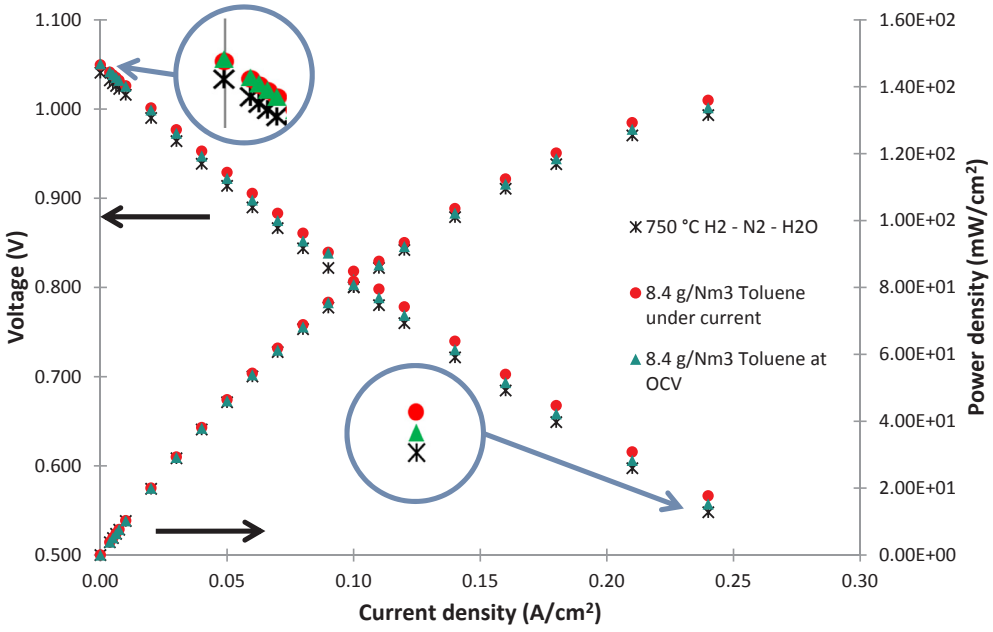

Fig. 6. Polarisation and power density curves of the cell operating at 750 °C before and after 60 min with 8.4 g/Nm^3 toluene at OCV and under 0.08 A/cm^2 current.

carbon [48].

Table 6 shows the flow rates measured at the outlet of the setup during the tests. An increase in toluene amount resulted in a higher content of the compounds formed during its conversion. However, the higher the toluene content, the lower the ratio between outlet and inlet molar flow of carbon, which decreased from more than 80% with 2.5 g/Nm^3 to 65% with 8.4 g/Nm^3 toluene, as illustrated in Fig. 9. This is in accordance with the observed increased deviation between expected and measured OCV. This might be due to a higher amount of toluene passing through the anode without any effect or, as previously explained, to the less accurate assumption of equilibrium between toluene liquid and gaseous phase. The inlet carbon molar flow was calculated from the assumed inlet toluene molar flow; the outlet carbon molar flow is the sum of CO, CO_2 and CH_4 molar flows, but it does not include toluene or other tar compounds. Moreover, despite no degradation of cell was observed, the deposition of solid carbon on the cell or in other parts of the setup cannot be excluded with certainty and further research is required.

When fed with a concentration of toluene up to 8.4 g/Nm^3, the cell did not show signs of degradation if operated under current or at OCV. The measured OCV was lower than the calculated Nernst potential and the carbon molar flow rate at the outlet was noticeably less than the inlet flow rate. Therefore, the tar seems to be partially reformed and oxidised inside the cell anode.

The possibility to directly reform toluene in the SOFC anode is an opportunity for decreasing system complexity. The external tar reformer might in fact be not necessary if tar compounds can be reformed internally. The results is also interesting for systems with cold gas cleaning systems since toluene is more difficult to remove than heavier compounds.

3.3. Combined effect of tar and HCl

Table 7 presents the variations in ASR due to the combined presence of 8.4 g/Nm^3 toluene and an increasing amount of HCl. When the cell was kept at OCV, the combined presence of 8.4 g/Nm^3 toluene and 8–82 ppmv HCl caused the ASR to increase by roughly 1–1.5%. Differently from the case with HCl alone, the addition of 8.4 g/Nm^3 toluene caused the ASR to increase even with only 8 ppmv HCl. Fig. 10 presents polarisation and power density curves after 60 min exposure at OCV to simultaneously 8.4 g/Nm^3 toluene and 82 ppmv HCl. The presence of toluene increased the cell voltage indicating the occurrence of reforming even if HCl was present. As in the previous cases, the ASR decreased as compared to the reference test after keeping the cell under current. However, this was observed only for the two lowest HCl concentrations. In fact, with 82 ppmv HCl the ASR resulted marginally higher than in the reference case even after keeping the cell under current. This is similar to what observed when the cell was fed only with HCl. Also in this case, this minor performance drop was observed right upon the addition of the contaminants and did not become more severe with time. As previously mentioned for the case of HCl alone and as reported by Trembly et al. [43], the simultaneous presence of adsorbed HCl and toluene might lead to a decrease in the Ni active sites available for H_2 oxidation.

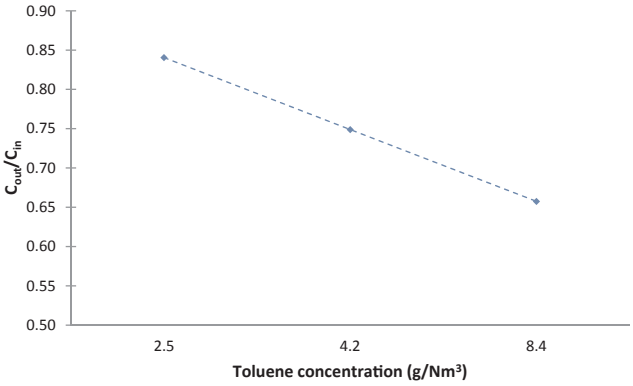

Fig. 9. Percentage ratio of outlet and inlet carbon molar flow when the cell was kept at OCV.

Table 7
ASR variation when 8.4 g/Nm^3 toluene and an increasing amount of HCl are added to the anode gas, after 60 min of exposure at OCV and under current.

HCl concentration (ppmv)	ASR deviation after 60 min at OCV (%)	ASR deviation after 60 min@0.08 A/cm^2 (%)
8	1.1	−1.4
42	1.6	−0.7
82	1.5	0.7

When HCl was fed together with toluene, the outlet flow rates of CO_2 and CO decreased. Even low concentrations of HCl seemed to affect tar reforming. Table 8 presents the outlet flow rates. In the same table, the ratio between the carbon molar flow rate at the outlet and at the inlet is shown. There was no much difference between the effect of 8 and 42 ppmv, which both decreased the carbon ratio of around 6 percentage points with respect to the case without HCl. However, 82 ppmv HCl caused a significant drop in the outlet carbon molar flow rate. The ratio between outlet and inlet carbon molar flows reached only around 50% when 82 ppmv HCl were present. The results collected indicate a clear influence of HCl on the reactions involving toluene in the anode chamber, in accordance with what observed by Reeping et al. with CH_4 as fuel [35].

Summarising, the simultaneous presence of toluene and HCl caused a marginal increase in the ASR even at HCl concentrations as low as 8 ppmv. However, this increase was lower than 2% and did not become more severe with time. The results collected indicate an influence of HCl on the reactions involving toluene in the anode chamber.

Despite the cell appeared not to be significantly affected by 8 ppmv HCl alone, it appears it is necessary to lower HCl concentrations below this value if the system is designed with direct internal reforming. HCl concentration below 1 ppmv can be obtained at temperature as high as 500 °C. Further research on the cross-influence effect with very low concentrations of HCl is however required. Cross-influence studies are fundamental for system development. The results of HCl and toluene

Table 6
Outlet flow rates measured with increasing concentration of toluene when the cell was kept at OCV and under current.

Measured outlet flow rate (NmL/min)							
	Reference OCV	2.5 g/Nm^3 OCV	2.5 g/Nm^3 current	4.2 g/Nm^3 OCV	4.2 g/Nm^3 current	8.4 g/Nm^3 OCV	8.4 g/Nm^3 current
H_2	436.72	438.08	399.20	441.50	403.12	448.08	411.43
N_2	889.98	889.98	889.98	885.11	885.11	872.96	872.96
CH_4	0.00	0.11	0.05	0.21	0.10	0.53	0.31
CO	0.00	3.41	3.21	5.73	5.28	10.96	10.50
CO_2	0.00	1.63	1.66	1.70	1.95	1.93	2.42
Tot.	1326.69	1333.21	1294.10	1334.26	1295.56	1334.47	1297.63

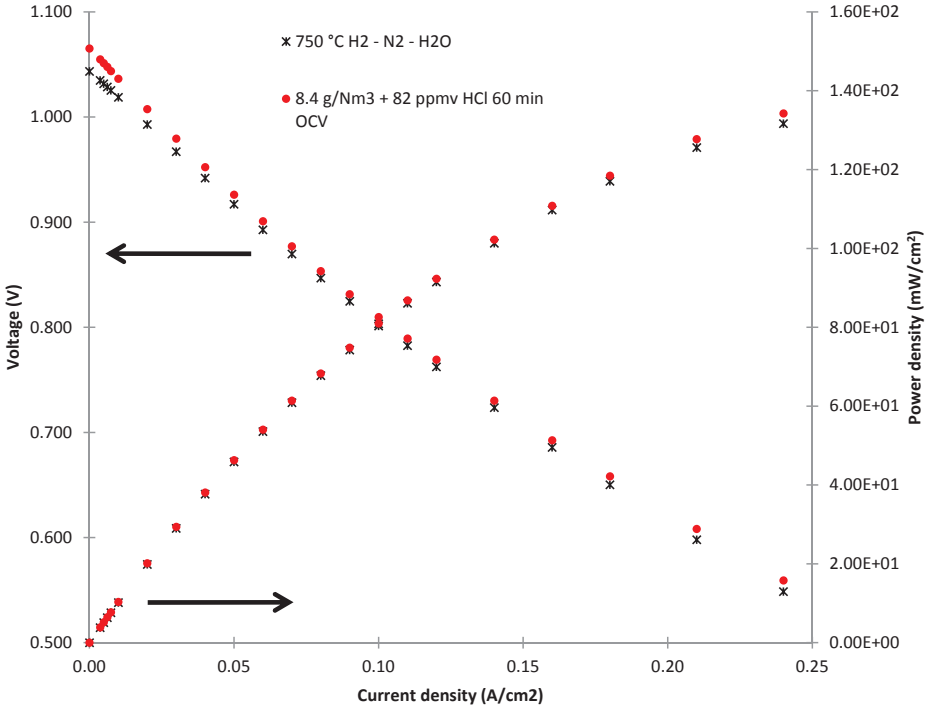

Fig. 10. Polarisation and power density curves of the cell operating at 750 °C before and after 60 min with 8.4 g/Nm^3 toluene and 42 ppmv HCl at OCV.

Table 8
Outlet flow rates measured with 8.4 g/Nm^3 toluene and increasing concentration of HCl when the cell was kept at OCV and under current.

Measured outlet flow rate (NmL/min)								
HCl	0 ppmv OCV	0 ppmv current	8 ppmv OCV	8 ppmv current	42 ppmv OCV	42 ppmv current	82 ppmv OCV	82 ppmv current
H_2	448.08	411.43	446.85	409.99	452.56	415.30	443.27	405.22
N_2	872.96	872.96	872.96	872.96	872.96	872.96	872.96	872.96
CH_4	0.53	0.31	0.53	0.31	0.66	0.36	0.42	0.24
CO	10.96	10.50	9.88	9.88	9.88	9.57	8.59	8.47
CO_2	1.93	2.42	1.76	2.26	1.74	2.21	1.59	2.07
Tot.	1334.47	1297.63	1331.99	1295.41	1337.81	1300.40	1326.83	1288.98
Cout/Cin	66%	65%	60%	61%	60%	59%	52%	53%

separately might lead to the conclusion that toluene is internally reformed and that SOFC tolerance limit of HCl is above 10 ppmv. However, when a system is designed with direct internal tar reforming, the results of this study indicate that HCl concentration should be lowered below few ppmv.

3.4. Observations and future work

When toluene was introduced in the anode flow, besides CO and CO_2, also CH_4 was measured at the outlet of the setup and its amount increased with increasing inlet concentration of toluene. Table 9 shows the calculated equilibrium outlet gas composition when 8.4 g/Nm^3 toluene were introduced.

The presence of methane was expected if equilibrium conditions were achieved. However, the formation pathway of methane is not known. Mermelstein et al. observed CH_4 formation while reforming benzene carried by humidified H_2 over Ni-YSZ and Ni-GDC. They concluded that the methane was formed via methanation since benzene remains adsorbed with steam on the Ni catalyst until all the carbon atoms are converted to CO or CO_2, as suggested also by Coll et al. [12,39]. Methanation might also be the origin of CH_4 observed in our tests. However, toluene and benzene have a very different structure with the former presenting a methyl group attached to the phenyl group which might be the responsible for the presence of methane [49]. Moreover, formation of methane from toluene in hydrogen atmosphere and more in general from tar reforming has been previously reported in literature [50,51]. This pathway might also explain the observed effect of HCl on CH_4 concentration. When 42 ppmv HCl were present, an increase in the CH_4 content was observed. This might have been caused by HCl preventing the methane generated from the methyl group to be reformed. When HCl concentration is increased to 82 ppmv, even the adsorption of toluene on Ni is possibly hindered, thus preventing the release of the methyl groups and the formation of methane. Further research is required to understand the mechanism responsible for the observed CH_4 behaviour, and the hindering of reforming caused by the presence of HCl. Electrochemical Impedance Spectroscopy (EIS) and

Table 9
Comparison between measured and equilibrium gas composition at cell outlet with 8.4 g/Nm^3 toluene.

	Equilibrium composition (vol% dry basis)	Measured concentration (vol% dry basis)
H_2	36.42	33.58
N_2	62.12	65.42
CH_4	0.05	0.04
CO	1.28	0.82
CO_2	0.13	0.14

post-mortem analysis with Scanning Electron Microscope and Energy Dispersive X-ray Spectroscopy (SEM-EDS) are suggested for a more detailed understanding of the mechanism behind the observations reported in this work. Moreover, the concentration of toluene should be measured at the cell outlet to properly quantify the extent of reforming taking place in the anode chamber.

The results obtained on the effect of HCl should be extended with long term tests using biosyngas. The contaminant might in fact compete with the other biosyngas compounds for the Ni active sites and worsen the cell degradation rate. For what concerns tar, despite toluene is the most abundant tar species generated in downdraft gasifiers, and it is more reactive than polyaromatic tar compounds, long term tests using real tar from gasifiers and biosyngas are suggested. Moreover, since HCl seems to affect reforming, degradation might appear in long-term tests due to fuel starvation close to the anode outlet. These tests are recommended before coming up with final gas cleaning unit designs for Integrated Biomass Gasifier SOFC Systems.

4. Conclusions

This work is part of a series of studies undertaken in order to improve the design of Integrated Biomass Gasifier Solid Oxide Fuel Cell Systems by generating detailed understanding of the cross-influence of HCl and toluene as a model tar on Solid Oxide Fuel Cell. With present days knowledge, in these systems tar compounds are removed or reformed externally since no complete understanding of their fate in Solid Oxide Fuel Cell anode is available in literature. For what concerns HCl, its concentration is decreased in the ppmv range. However, tolerance limits used in designing gas cleaning units for gasifier-Solid Oxide Fuel Cell systems are based on single contaminants effects. This might result in incorrect understanding of Solid Oxide Fuel Cell tolerance limits, and improper design of the system gas cleaning unit. Therefore, experiments were carried out to evaluate the possibility of reforming tar internally, the synergistic effect of HCl and toluene as model tar on cell performances, and the effect of HCl on direct internal tar reforming.

The highest concentration of HCl tested, 82 ppmv, caused only a marginal increase in the cell ASR (around 1.5% when the cell was operated at Open Circuit). However, the Area Specific Resistance then remained constant during the exposure time. This amount of HCl is therefore believed not to significantly affect Ni-GDC anodes when fed with H_2. Concentrations of toluene up to 8.4 g/Nm^3 did not cause performance degradation. Toluene seems to be partially reformed and oxidised inside the cell anode. When toluene and HCl are simultaneously present, a marginal increase in the ASR was observed even at HCl concentrations as low as 8 ppmv. However, this increase was lower than 2% and remained then constant during the exposure. Nonetheless, HCl seemed to partially hinder toluene conversion in the anode chamber, even at low concentration.

The results obtained give a useful insight in the interaction between HCl, tar, and the cell anode material. HCl seems not to be a deleterious contaminant at the concentrations tested, thus indicating the possibility of simplifying the system gas cleaning unit. Also the possibility to reform toluene internally in the Solid Oxide Fuel Cell represent an opportunity to further decrease system complexity. However, even if the simultaneous presence of the two contaminants does not significantly damage the cell, HCl influences direct internal tar reforming. The system gas cleaning unit should be therefore designed keeping in mind that tolerance limits differ depending on what are the reactions expected to occur in the Solid Oxide Fuel Cell.

The exposure time in these tests was very short, and the gas composition used was a mixture of H_2 and N_2 as opposed to biosyngas, where these contaminants are usually found. Therefore, the feasibility of direct internal tar reforming and the influence of HCl have to be studied in detail by long term tests using biosyngas as tar gas carrier and real tar from gasifiers. Extensive studies are required before coming up with final gas cleaning unit designs for systems with direct internal reforming. Studying contaminants cross-influence is fundamental to assure safe and efficient operation of Integrated Biomass Gasifier Solid Oxide Fuel Cell Systems.

Acknowledgment

This research is partially supported by the project “FlexiFuel-SOFC”. The project has received funding from the European Union’s Horizon 2020 research and innovation programme under grant agreement No. 641229. The authors acknowledge the preliminary work done during the internship of Y.H. Liu, supervised by Dr. M. Liu and Dr. P. V. Aravind.

References

[1] Caposciutti G, Barontini F, Antonelli M, Tognotti L, Desideri U. Experimental investigation on the air excess and air displacement influence on early stage and complete combustion gaseous emissions of a small scale fixed bed biomass boiler. Appl Energy 2018;216:576–87. https://doi.org/10.1016/j.apenergy.2018.02.125.
[2] Cinti G, Desideri U. SOFC fuelled with reformed urea. Appl Energy 2015;154:242–53. https://doi.org/10.1016/j.apenergy.2015.04.126.
[3] Bocci E, Di Carlo A, McPhail SJ, Gallucci K, Foscolo PU, Moneti M, et al. Biomass to fuel cells state of the art: a review of the most innovative technology solutions. Int J Hydrogen Energy 2014;39:21876–95. https://doi.org/10.1016/j.ijhydene.2014.09.022.
[4] Abdoulmoumine N, Adhikari S, Kulkarni A, Chattanathan S. A review on biomass gasification syngas cleanup. Appl Energy 2015;155:294–307. https://doi.org/10.1016/j.apenergy.2015.05.095.
[5] Pumiglia D, Vaccaro S, Masi A, McPhail SJ, Falconieri M, Gagliardi S, et al. Aggravated test of Intermediate temperature solid oxide fuel cells fed with tar-contaminated syngas. J Power Sources 2017;340:150–9. https://doi.org/10.1016/j.jpowsour.2016.11.065.
[6] Aravind PV, de Jong W. Evaluation of high temperature gas cleaning options for biomass gasification product gas for Solid Oxide Fuel Cells. Prog Energy Combust Sci 2012;38:737–64. https://doi.org/10.1016/j.pecs.2012.03.006.
[7] Singh D, Hernández-Pacheco E, Hutton PN, Patel N, Mann MD. Carbon deposition in an SOFC fueled by tar-laden biomass gas: a thermodynamic analysis. J Power Sources 2005;142:194–9. https://doi.org/10.1016/j.jpowsour.2004.10.024.
[8] Mermelstein J, Millan M, Brandon N. The impact of steam and current density on carbon formation from biomass gasification tar on Ni/YSZ, and Ni/CGO solid oxide fuel cell anodes. J Power Sources 2010;195:1657–66. https://doi.org/10.1016/j.jpowsour.2009.09.046.
[9] Papurello D, Lanzini A, Leone P, Santarelli M. The effect of heavy tars (toluene and naphthalene) on the electrochemical performance of an anode-supported SOFC running on bio-syngas. Renew Energy 2016;99:747–53. https://doi.org/10.1016/j.renene.2016.07.029.
[10] Hauth M, Lerch W, König K, Karl J. Impact of naphthalene on the performance of SOFCs during operation with synthetic wood gas. J Power Sources 2011;196:7144–51. https://doi.org/10.1016/j.jpowsour.2010.09.007.
[11] Aravind PV, Ouweltjes JP, Woudstra N, Rietveld G. Impact of biomass-derived contaminants on SOFCs with Ni/gadolinia-doped ceria anodes. Electrochem Solid-State Lett 2008;11:B24. https://doi.org/10.1149/1.2820452.
[12] Mermelstein J, Brandon N, Millan M. Impact of steam on the interaction between biomass gasification tars and nickel-based solid oxide fuel cell anode materials. Energy Fuels 2009;23:5042–8. https://doi.org/10.1021/ef900426g.
[13] Mermelstein J, Millan M, Brandon NP. The impact of carbon formation on Ni-YSZ anodes from biomass gasification model tars operating in dry conditions. Chem Eng Sci 2009;64:492–500. https://doi.org/10.1016/j.ces.2008.09.020.
[14] Lorente E, Millan M, Brandon NP. Use of gasification syngas in SOFC: impact of real tar on anode materials. Int J Hydrogen Energy 2012;37:7271–8. https://doi.org/10.1016/j.ijhydene.2011.11.047.
[15] Lorente E, Berrueco C, Millan M, Brandon NP. Effect of tar fractions from coal gasification on nickel-yttria stabilized zirconia and nickel-gadolinium doped ceria solid oxide fuel cell anode materials. J Power Sources 2013;242:824–31. https://doi.org/10.1016/j.jpowsour.2013.05.158.
[16] Hofmann P, Panopoulos KD, Aravind PV, Siedlecki M, Schweiger A, Karl J, et al. Operation of solid oxide fuel cell on biomass product gas with tar levels > 10 g Nm^{-3}. Int J Hydrogen Energy 2009;34:9203–12. https://doi.org/10.1016/j.ijhydene.2009.07.040.
[17] Hofmann P, Panopoulos KD, Fryda LE, Schweiger A, Ouweltjes JP, Karl J. Integrating biomass gasification with solid oxide fuel cells: effect of real product gas tars, fluctuations and particulates on Ni-GDC anode. Int J Hydrogen Energy 2008;33:2834–44. https://doi.org/10.1016/j.ijhydene.2008.03.020.
[18] Baldinelli A, Cinti G, Desideri U, Fantozzi F. Biomass integrated gasifier-fuel cells: Experimental investigation on wood syngas tars impact on NiYSZ-anode Solid Oxide Fuel Cells. Energy Convers Manage 2016;128:361–70. https://doi.org/10.1016/j.enconman.2016.09.048.
[19] Madi H, Diethelm S, Ludwig C, Van herle J. The impact of toluene on the performance of anode-supported Ni-YSZ sofc operated on hydrogen and biosyngas. ECS Trans 2015;68:2811–8. https://doi.org/10.1149/06801.2811ecst.
[20] Liu M, Millan-Agorio MG, Aravind PV, Brandon NP. Influence of operation

conditions on carbon deposition in SOFCs fuelled by tar-containing biosyngas 2011;158:2701–2712. http://doi.org/10.1149/1.3570269.
[21] Papurello D, Lanzini A, Drago D, Leone P, Santarelli M. Limiting factors for planar solid oxide fuel cells under different trace compound concentrations. Energy 2016;95:67–78. https://doi.org/10.1016/j.energy.2015.11.070.
[22] Papurello D, Iafrate C, Lanzini A, Santarelli M. Trace compounds impact on SOFC performance: experimental and modelling approach. Appl Energy 2017;208:637–54. https://doi.org/10.1016/j.apenergy.2017.09.090.
[23] Liu M, van der Kleij A, Verkooijen AHM, Aravind PV. An experimental study of the interaction between tar and SOFCs with Ni/GDC anodes. Appl Energy 2013;108:149–57. https://doi.org/10.1016/j.apenergy.2013.03.020.
[24] Doyle TS, Dehouche Z, Aravind PV, Liu M, Stankovic S. Investigating the impact and reaction pathway of toluene on a SOFC running on syngas. Int J Hydrogen Energy 2014;39:12083–91. https://doi.org/10.1016/j.ijhydene.2014.05.148.
[25] Namioka T, Naruse T, Yamane R. Behavior and mechanisms of Ni/ScSZ cermet anode deterioration by trace tar in wood gas in a solid oxide fuel cell. Int J Hydrogen Energy 2011;36:5581–8. https://doi.org/10.1016/j.ijhydene.2011.01.165.
[26] Chun CM, Mumford JD, Ramanarayanan TA. Carbon-induced corrosion of nickel anode. J Electrochem Soc 2000;147:3680. https://doi.org/10.1149/1.1393958.
[27] Marina OA, Pederson LR, Thomsen EC, Coyle CA, Yoon KJ. Reversible poisoning of nickel/zirconia solid oxide fuel cell anodes by hydrogen chloride in coal gas. J Power Sources 2010;195:7033–7. https://doi.org/10.1016/j.jpowsour.2010.05.006.
[28] Xu C, Gong M, Zondlo JW, Liu X, Finklea HO. The effect of HCl in syngas on Ni-YSZ anode-supported solid oxide fuel cells. J Power Sources 2010;195:2149–58. https://doi.org/10.1016/j.jpowsour.2009.09.079.
[29] Bao J, Krishnan GN, Jayaweera P, Sanjurjo A. Effect of various coal gas contaminants on the performance of solid oxide fuel cells: Part III. Synergistic effects. J Power Sources 2010;195:1316–24. https://doi.org/10.1016/j.jpowsour.2009.09.018.
[30] Haga K, Shiratori Y, Ito K, Sasaki K. Chlorine poisoning of SOFC Ni-Cermet anodes. J Electrochem Soc 2008;155:B1233. https://doi.org/10.1149/1.2980521.
[31] Trembly JP, Gemmen RS, Bayless DJ. The effect of coal syngas containing HCl on the performance of solid oxide fuel cells: Investigations into the effect of operational temperature and HCl concentration. J Power Sources 2007;169:347–54. https://doi.org/10.1016/j.jpowsour.2007.03.018.
[32] Kuramoto K, Hosokai S, Matsuoka K, Ishiyama T, Kishimoto H, Yamaji K. Degradation behaviors of SOFC due to chemical interaction between Ni-YSZ anode and trace gaseous impurities in coal syngas. Fuel Process Technol 2017;160:8–18. https://doi.org/10.1016/j.fuproc.2017.02.009.
[33] Li TS, Xu C, Chen T, Miao H, Wang WG. Chlorine contaminants poisoning of solid oxide fuel cells. J Solid State Electrochem 2011;15:1077–85. https://doi.org/10.1007/s10008-010-1166-x.
[34] Błesznowski M, Jewulski J, Zieleniak A. Determination of H2S and HCl concentration limits in the fuel for anode supported SOFC operation. Cent Eur J Chem 2013;11:960–7. https://doi.org/10.2478/s11532-013-0228-1.
[35] Reeping KW, Kirtley JD, Bohn JM, Steinhurst DA, Owrutsky JC, Walker RA. Chlorine-induced degradation in Solid Oxide Fuel Cells Identified by *Operando* optical methods. J Phys Chem C 2017;121:2588–96. https://doi.org/10.1021/acs.jpcc.6b11548.
[36] Madi H, Lanzini A, Papurello D, Diethelm S, Ludwig C, Santarelli M, et al. Solid oxide fuel cell anode degradation by the effect of hydrogen chloride in stack and single cell environments. J Power Sources 2016;326:349–56. https://doi.org/10.1016/j.jpowsour.2016.07.003.
[37] Cayan FN, Zhi M, Pakalapati SR, Celik I, Wu N, Gemmen R. Effects of coal syngas impurities on anodes of solid oxide fuel cells. J Power Sources 2008;185:595–602. https://doi.org/10.1016/j.jpowsour.2008.06.058.
[38] Milne T, Abatzoglou N, Evans R. Biomass gasifier “tars”: their nature, formation, and conversion. Colorado; 1997.
[39] Coll R, Salvadó J, Farriol X, Montané D. Steam reforming model compounds of biomass gasification tars: Conversion at different operating conditions and tendency towards coke formation. Fuel Process Technol 2001;74:19–31. https://doi.org/10.1016/S0378-3820(01)00214-4.
[40] Thermfact/CRCT, GTT-Technologies. FactSage n.d. www.factsage.com.
[41] Zeisler J, Kleinhappl M, Hofbauer H. Reliable sampling of impurities in product gas and syngas 2010:1–12.
[42] Botta G, Solimeo M, Leone P, Aravind PV. Thermodynamic analysis of coupling a SOEC in co-electrolysis mode with the dimethyl ether synthesis. Fuel Cells 2015;15:669–81. https://doi.org/10.1002/fuce.201500016.
[43] Trembly JP, Gemmen RS, Bayless DJ. The effect of coal syngas containing AsH3 on the performance of SOFCs: investigations into the effect of operational temperature, current density and AsH3 concentration. J Power Sources 2007;171:818–25. https://doi.org/10.1016/j.jpowsour.2007.06.087.
[44] Van Der Drift A, Van Doorn J, Vermeulen JW. Ten residual biomass fuels for circulating gasiÿcation. Biomass Bioenergy 2001;20:45–56. https://doi.org/10.1016/S0961-9534(00)00045-3.
[45] Stemmler M, Müller M. Chemical hot gas cleaning concept for the “CHRISGAS” process. Biomass Bioenergy 2011;35.. https://doi.org/10.1016/j.biombioe.2011.03.044.
[46] Krishnan GN, Gupta RP, Canizales A, Shelukar S, Ayala RE. Removal of hydrogen chloride from hot coal gas streams. High Temp Gas Clean 1996;1:405–14.
[47] Mallon C, Kendall K. Sensitivity of nickel cermet anodes to reduction conditions. J Power Sources 2005;145:154–60. https://doi.org/10.1016/j.jpowsour.2005.02.043.
[48] Daza CE, Kiennemann A, Moreno S, Molina R. Dry reforming of methane using Ni-Ce catalysts supported on a modified mineral clay. Appl Catal A Gen 2009;364:65–74. https://doi.org/10.1016/j.apcata.2009.05.029.
[49] Emdee JL, Brezinsky K, Glassman I. A kinetic model for the oxidation of toluene near 1200 K. J Phys Chem 1992;96:2151–61. https://doi.org/10.1021/j100184a025.
[50] Saroğlan A. Tar removal on dolomite and steam reforming catalyst: benzene, toluene and xylene reforming. Int J Hydrogen Energy 2012;37:8133–42. https://doi.org/10.1016/j.ijhydene.2012.02.045.
[51] Zimmerman CC, York R. Thermal demethylation of toluene. Ind Eng Chem Process Des Dev 1964;3:254–8. https://doi.org/10.1021/i260011a013.